Metal Nanodendrites

DOI: 10.1002/ange.201205956

Manipulating Local Ligand Environments for the Controlled Nucleation of Metal Nanoparticles and their Assembly into Nanodendrites**

*Nancy Ortiz and Sara E. Skrabalak**

One could argue that the synthesis of metal nanostructures with well-defined features remains an art, not a science, given our current understanding of how metal precursors are transformed into small metal clusters and eventually larger nanostructures. Here, we report a facile route to palladium nanodendrites and larger Pd bundles through the thermal decomposition of Pd precursors in only oleylamine. This simple, two-component system was designed to evaluate the effect of the local ligand environment on the nucleation of nanoparticles and their subsequent growth through either atomic addition or aggregation. It was found that both the nucleation and growth stages associated with the formation of the nanostructures, and thus the final morphologies, were controlled by the binding affinity of the ligands. Significantly, our analysis connects the formation of nanostructures directly to fundamental principles of coordination chemistry and provides universal guidelines that can be applied to the synthesis of other dendritic structures and high-quality nanomaterials in general. In particular, it was found that ligands with intermediate binding affinity towards Pd^{II} ions regulate their gradual reduction and promote the aggregation-based assembly of the weakly passivated Pd nanoparticles into nanodendrites. In contrast, strongly coordinated ligands delay burst-like nucleation, and growth of quasispherical well-passivated nanoparticles through atomic addition is favored. As metal nanostructures with branched morphologies often display distinct physicochemical properties, extracting the crucial parameters governing their formation will contribute to the future synthesis of structurally distinct metal dendrites. As we found, the principles that guided the ligand-controlled synthesis of Pd dendrites were general and also enabled the synthesis of Pt nanodendrites.

Typical methods for producing nanoparticles composed of face-centered cubic (fcc) metals yield polyhedral shapes favored by thermodynamics; however, different growth mechanisms such as kinetically controlled overgrowth, aggregation-based growth, and template-mediated methods can be employed to synthesize branched metal nanoparticles in solution.[1] For example, Pt-on-Pd nanodendrites with superior catalytic activity for oxygen reduction were produced by using preformed Pd cuboctahedra as templates for the subsequent dendritic growth of Pt.[2] In this case, dendritic growth was attributed to a high rate of reduction for the Pt precursor facilitated by a seed-mediated autocatalytic process. Similar overgrowth processes have been reported in other syntheses of metal dendrites and are often coupled with the in situ generation of seeds.[3] Interestingly, Tilley and coworkers verified the importance of rapid growth kinetics in the formation of branched metal nanoparticles by monitoring the synthesis of Pd dendrites from $PdCl_2{\cdot}(CH_3CN)_2$ in the presence of toluene, oleylamine, oleic acid, and H_2 by an in situ synchrotron X-ray diffraction (XRD) technique.[4] The significance of nucleation and growth rates on the formation of branched nanoparticles was further demonstrated by Xia

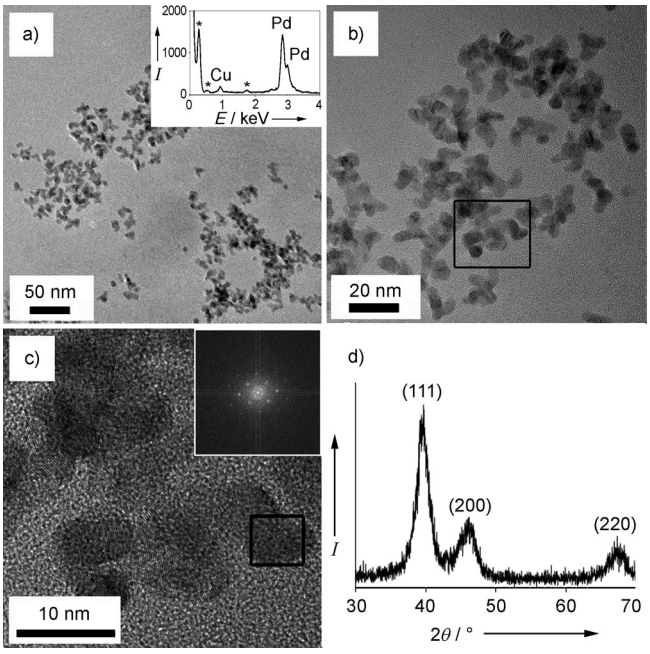

Figure 1. Characterization of Pd nanodendrites synthesized by the reduction of $[Pd(acac)_2]$ in the presence of oleylamine: a) TEM image and corresponding EDX analysis (inset); the Cu signal arises from the TEM grid, and * denotes signals from the sample holder; b) higher magnification TEM image of (a); c) high-resolution TEM image of the selected area denoted in (b), with the FFT (inset) of the selected area in (c); and d) powder XRD pattern of Pd nanodendrites.

[*] N. Ortiz, Dr. S. E. Skrabalak
Indiana University, Department of Chemistry
800 E. Kirkwood, Bloomington, IN, 47405-7102 (USA)
E-mail: sskrabal@indiana.edu
Homepage: http://www.indiana.edu/~skrablab/

[**] This work was supported by Indiana University and the Cottrell Scholar Program sponsored by the Research Corporation for Science Advancement. We thank Dr. David Morgan of the IU Nanoscale Characterization Facility for assistance with TEM measurements, and Dr. Maren Pink of the IU Molecular Structure Center for assistance with XRD measurements.

Supporting information for this article is available on the WWW under http://dx.doi.org/10.1002/anie.201205956.

and co-workers with the synthesis of Pt nanodendrites; however, in this example, dendrite formation was facilitated by self-aggregation of small Pt particles, not an overgrowth process.[5] Specifically, 3 nm Pt particles were initially formed which assembled into polycrystalline dendritic structures. The formation of branched nanostructures through aggregation is often misassigned and is typically observed among small particles where the collision-stick frequency is greatest and driven by their high kinetic energy and a reduction in surface energy upon the attachment of particles.[6] The architecture of the final nanodendrites is governed by the concentration of nanoparticles in solution and their mobility, with open structures consistent with diffusion-limited aggregation observed under dilute conditions.[1a] Often, intricate synthetic conditions or reliance on multiple synthetic steps and constituents make it difficult to predictably select precursors and reaction conditions to achieve nanodendrites by these established growth mechanisms. Through our systematic variation of a two-component system comprised of a Pd precursor and oleylamine, we have found that the formation of metal dendrites through aggregation-based growth is linked to weak ligand interactions to both Pd^{II} ions and the generated Pd nanoparticles.

Specifically, palladium acetylacetonate ($[Pd(acac)_2]$) was employed as a Pd precursor, and oleylamine served as both the capping agent and solvent. In the optimized synthesis, this solution was heated in an argon atmosphere from room temperature to 130 °C at a rate of about 20 °C min^{-1}. Notably, this synthesis is the first report which circumvents the use of preformed seeds as nucleation sites, numerous synthesis components, and/or multiple synthetic steps for the formation of nanodendrites in an organic medium. Figure 1 shows the characterization of the Pd nanodendrites which form within 10 minutes of heating. Analysis by transmission electron microscopy (TEM) reveals the formation of Pd nanostructures with branched morphology 10 to 20 nm across and composed of smaller spherical crystallites with diameters of about 4 nm (Figure 1 a–c). High-resolution TEM and fast-Fourier transforms (FFTs) of the individual crystallite regions highlight their single-crystalline nature (Figure 1 c, inset), but the overall nanodendrite is polycrystalline. Different lattice orientations are apparent, and adjacent FFTs display different patterns and/or orientations (see Figure S1 in the Supporting Information). This structural analysis is consistent with misorientation at particle interfaces and is characteristic of polycrystalline branched nanoparticles formed through aggregation-based growth, not overgrowth (where continuous lattice fringes and identical FFTs are indicative of an epitaxial relationship between features).[2] Energy-dispersive X-ray (EDX) spectroscopy confirmed the presence of Pd (Figure 1 a, inset), which was further substantiated by powder XRD (Figure 1 d). The XRD pattern exhibits three reflections which are consistent with the {111}, {200}, and {220} indices of fcc Pd. The average crystallite size was calculated from the Scherrer equation to be 4.37 nm by using the full-width at half-maximum of the {111} reflection. This value is consistent with the high-resolution TEM analysis (Figure 1 c) and the discrete Pd particles formed in the early stages of the reaction (see Figure S2 in the Supporting Information).

The formation of the Pd nanodendrites by aggregation-based growth was further substantiated by TEM analysis and UV/Vis spectroscopy of reaction aliquots as a function of time (Figure 2 and Figure S2 in the Supporting Information). Nanodendrites are observed within five minutes; however, the sample consists predominately of discrete particles < 5 nm in diameter. This particle size is on the same scale as the individual crystallites which comprise the dendritic structures. Only a small percentage of discrete Pd nanoparticles are observed at longer times, and by six hours the Pd dendrites have evolved into larger, porous bundles 100–200 nm across (Figure 2 a). UV/Vis spectroscopic analysis of this growth process revealed the gradual reduction of the Pd precursor (Figure 2 b). At $t = 0$, one absorbance feature is observed at about 278 nm which has been identified as a $[Pd(acac)_2]$–oleylamine complex (see Figure S3 in the Supporting Information). The intensity of this feature gradually decreased with reaction time, as a secondary absorbance

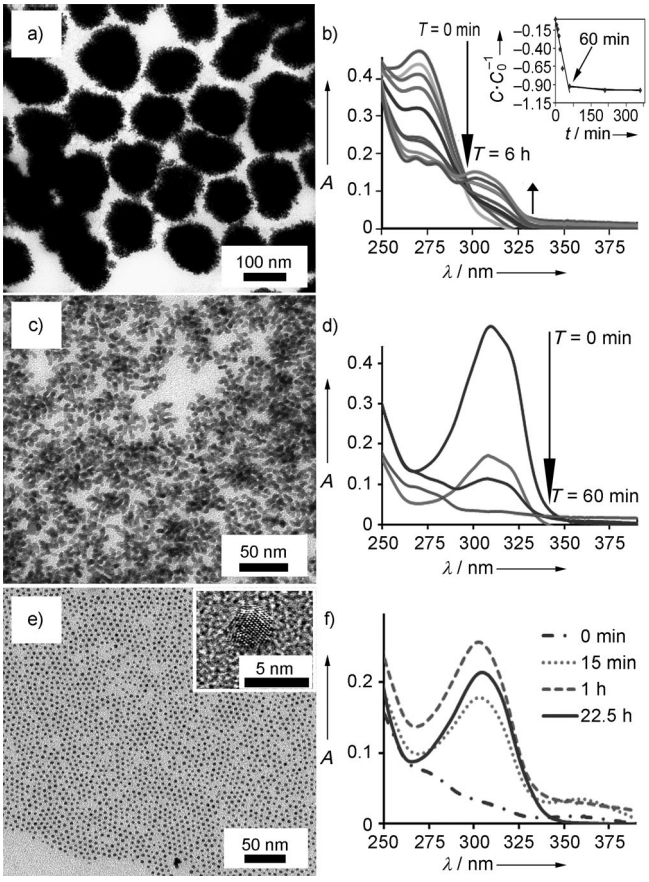

Figure 2. Comparison of nanoparticle morphology and induction time by TEM and analysis by UV/Vis spectroscopy, respectively: a) TEM image of Pd bundles produced after 6 h of heating $[Pd(acac)_2]$ in oleylamine and b) corresponding analysis by UV/Vis spectroscopy of aliquots removed between 0 min and 6 h of reaction time (inset: change in precursor consumption rate); c) Pd nanodendrites formed by heating $[Pd(hfac)_2]$ in oleylamine for 6 h and d) analysis by UV/Vis spectroscopy of reaction aliquots removed between 0 min and 60 min; e) TEM image of single-crystalline spherical Pd nanoparticles prepared by heating $[Pd(acac)_2]$ in TOP and oleylamine for 22.5 h and f) corresponding analysis of the precursor consumption rate by UV/Vis spectroscopy of reaction aliquots removed between 0 min and 22.5 h.

appeared at about 310 nm and grows to a steady absorbance by six hours. The secondary absorbance likely corresponds to a side product from the release or internal oxidation of the $acac^-$ ligands, and also correlates with the generation of Pd^0. Between one and six hours, the rate of this process slows then ceases, marking the end of the reaction (Figure 2b, inset). Thus, Pd nuclei are continually supplied at a low concentration during the first hour of the growth process, which is predominated by the aggregation of discrete nanoparticles. In the later stages of the reaction when the small nanodendrites transform into larger bundles, the Pd precursor is highly depleted. Thus, the dramatic increase in the size of the nanostructures must arise by coalescence of the already formed dendrites rather than the generation of new nanoparticles. Remarkably, controlling the reaction temperature allows the nanostructures to be easily tuned between small (approximately 20 nm) dendrites and fully developed porous bundles, with the bundles accessed more rapidly at higher reaction temperatures (see Figure S4 in the Supporting Information).

Given the simplicity of this synthetic approach, the role of the precursor on nanodendrite formation, and in particular the local ligand environment, was investigated by replacing $[Pd(acac)_2]$ with palladium hexafluoroacetylacetonate ($[Pd(hfac)_2]$), palladium acetate ($Pd(OAc)_2$), or phase-transferred sodium tetrachloropalladate (Na_2PdCl_4) as the Pd source, but using otherwise identical reaction conditions. Interestingly, Pd dendrites were again generated in all cases (Figure 2c and Figure S5 in the Supporting Information); however, prolonged heating and higher temperatures did not facilitate the transformation of the small dendrites into larger bundles. To understand this difference, the reduction process associated with $[Pd(hfac)_2]$ was monitored by UV/Vis spectroscopy and revealed that the Pd precursor is essentially consumed within one hour of reaction. Thus, the lack of formation of larger bundles is likely the result of more effective electrostatic stabilization of the dendrites by the released counterions from the precursors, but the generation of more nuclei in the initial stages of the reaction from $[Pd(hfac)_2]$, $Pd(OAc)_2$, or phase-transferred Na_2PdCl_4 may also account for the change. Regardless, the formation of structurally similar Pd dendrites after approximately one hour of reaction from all the precursors is indicative of similar nucleation and growth processes, namely, aggregation-based assembly, and either small spherical nanoparticles or much smaller dendrites were observed in the earliest stages of reaction. It is also noted that all four precursors consist of square-planar Pd^{II} environments, and the mechanisms of reduction to Pd^0 are similar.[7] That is, for reduction of Pd^{II} to Pd^0 to occur, oleylamine must coordinate to the metal center through the amine functionality. In the case of Na_2PdCl_4, the phase-transfer process should facilitate the coordination of oleylamine to the Pd^{II} center. For $Pd(OAc)_2$, $[Pd(hfac)_2]$, and $[Pd(acac)_2]$, oleylamine can either adopt axial positions in equilibrium with free oleylamine or coordinate in-plane, as the bidentate ligands adopt monodentate coordination (see Figure S6 in the Supporting Information). Thus, the observance of similar nucleation and growth behaviors with these precursors is unsurprising. These observations also suggest that suppressing amine coordination will greatly delay reduction by altering the pathway by which the nanoparticles are generated.

To test this hypothesis, softer ligands with greater binding affinity for Pd^{II} ions such as trioctylphosphine (TOP) and triphenylphosphine (PPh_3) where added to the $[Pd(acac)_2]$–oleylamine system under otherwise identical conditions. These ligands were expected to displace any oleylamine coordinated to the Pd^{II} center, stabilize the complex, and delay nucleation and growth.[8] Indeed, the morphology of the final product was dramatically altered, with single-crystalline Pd nanoparticles of spherical morphology forming in the presence of TOP after 22.5 hours of heating (Figure 2e) and poorly defined Pd nanoparticles after about 2 days in the presence of PPh_3 (see Figure S7 in the Supporting Information). The reaction in which TOP was added was monitored by UV/Vis spectroscopy and confirmed the displacement of the amine reducing agent (Figure 2f, compare with reference spectra in Figure S3 in the Supporting Information).[7c] At $t = 0$, a weak absorbance at approximately 278 nm is observed and reminiscent of the $[Pd(acac)_2]$–oleylamine only solution. With heating, a signature peak at about 305 nm emerges which has been identified as a Pd^{II}–TOP intermediate (Figure 2f and Figure S3 in the Supporting Information). Reduction of Pd^{II} to Pd^0 should proceed by the facile amine-assisted pathway in the system with only oleylamine (see Figure S6 in the Supporting Information).[8] In contrast, a more stable intermediate forms when TOP is present, as reductive elimination or radical-assisted reduction are the likely pathways to Pd^0, as proposed by Hyeon and co-workers.[7c] Thus, the coordination of oleylamine to Pd^{II} centers is suppressed by the more favorable soft–soft interactions between the Pd^{II} centers and TOP, which has also been verified by Yang and Klabunde.[8] The Pd^{II}–TOP feature grows in absorbance when the reaction is heated, but at 22.5 hours a decrease in absorbance is observed, which corresponds with the onset of nanoparticle generation, as revealed by TEM measurements of reaction aliquots. This observation agrees with the concept of delayed nucleation described by Alivisatos and co-workers, which has also been examined by Hyeon and co-workers when studying the origin of monodisperse samples by "heat-up" methods.[9]

These results indicate that the addition of ligands with greater binding affinity for Pd^{II} ions delays the nucleation process by displacement of the reducing agent and the formation of a more-stable intermediate, denoted as PdL_2–PR_3 (see Figure S6 in the Supporting Information). However, these experiments with TOP and PPh_3 do not allow the role of the local ligand environment on nucleation to be completely decoupled from the growth. That is, the phosphine ligands will coordinate to the surfaces of the Pd nanoparticles more strongly than oleylamine, which could inhibit aggregation. In fact, Sun and co-workers recently observed a change in the crystallinity of Pd nanoparticles upon displacement of surface oleylamine by TOP.[10] Characterization by EDX spectroscopy of our Pd nanoparticles prepared in the presence of TOP indicate that they are well-passivated by the capping agent, with a feature at about 1.9 keV indicating phosphorus, while no nitrogen feature is revealed in the oleylamine only system

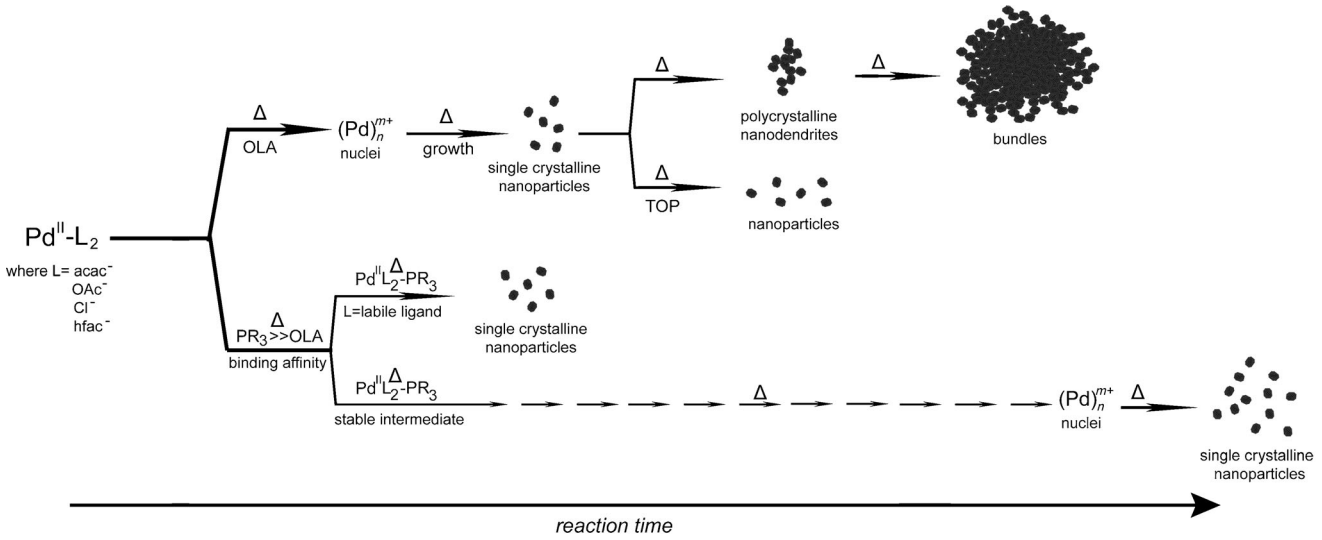

Figure 3. Scheme depicting the influence of ligand selection on the overall nucleation and growth processes for the formation of nanoparticles and nanodendrites. Weakly bound ligands, $acac^-$, OAc^-, Cl^-, and $hfac^-$, facilitated the formation of dendrites in the presence of oleylamine. The addition of TOP or PPh_3 creates a stable $Pd^{II}L_2$–PR_3 intermediate and thus prolongs the nucleation process.

(see Figure S7a in the Supporting Information). Thus, three additional studies (Figure 3) were conducted to better separate the roles of ligands on nucleation and growth.

The first study evaluated the effect of extraneous capping agent selection on the aggregation of the nanoparticles. TOP was injected into a solution of only $[Pd(acac)_2]$ and oleylamine after 30 min of reaction to determine whether or not its addition would suppress the aggregation of existing Pd nanoparticles and nanodendrites. Notably, the added TOP prevents the evolution of the nanodendrites into bundles, which is otherwise observed within six hours (see Figure S8 in the Supporting Information). In this case, a) the labile oleylamine is displaced by TOP to create the stable Pd^{II}–TOP intermediate with any unreduced Pd precursor (see Figure S8d in the Supporting Information) and b) further aggregation is inhibited by ligand exchange between surface-bound oleylamine and TOP. Discrete Pd nanoparticles form after heating for an additional 23 hours (see Figure S8c in the Supporting Information). In general, phosphine ligands should coordinate more strongly to Pd surfaces than amines; however, on account of the steric differences between various phosphine ligands, their surface packing will vary and could result in slightly different growth behavior. This feature may account for the slightly larger Pd nanoparticles produced by the use of PPh_3 compared to TOP.

The second study evaluated the role of reducing agent selection on nanoparticle aggregation. Borane *tert*-butylamine (BTB) complex was selected as a strong reducing agent suitable for inducing a burst of nucleation from $[Pd(acac)_2]$ dissolved in oleylamine, just as in the TOP system.[11] However, on account of the Lewis acidity associated with the borane, BTB and its by-products are not anticipated to coordinate strongly to the surface. In this case, spherical Pd nanoparticles about 10 nm in diameter are produced in seconds (see Figure S9a in the Supporting Information). Despite the absence of a strongly coordinating capping agent, appreciable aggregation of the nanoparticles does not occur. This observation may seem counterintuitive; however, the formation of branched nanostructures through aggregation typically occurs when particles are small and their collision-stick frequency is high. In this case, the selection of a strong reducing agent facilitates the more rapid formation of larger particles by atomic addition, wherein the driving force for attachment is diminished.

The third study evaluated the role of the local ligand environment on nucleation rate. Specifically, $[Pd(hfac)_2]$ was thermally decomposed in a solution containing both oleylamine and TOP. Remarkably, monodisperse Pd nanoparticles about 5 nm in diameter are produced in minutes, not in >20 hours as observed in the analogous $[Pd(acac)_2]$ system (see Figure S9b in the Supporting Information). In this case, the rapid generation of Pd nanoparticles can be attributed to the better leaving-group properties of the $hfac^-$ ligands compared to $acac^-$,[7d] which allow more facile access of oleylamine to the Pd^{II} center despite the presence of TOP. This result highlights the important role the local ligand environment plays in determining the rate of nanoparticle nucleation while simultaneously demonstrating the important role of extraneous capping agent in selecting for or inhibiting nanoparticle aggregation.

Understanding the formation of specific metal nanostructures is important as the final shape and adopted architecture contribute to their overall functionality. Here, we report that both the nature of nanoparticle nucleation and growth can be manipulated by the local ligand environment of the metal precursor and the selection of extraneous capping agents to provide control over the final morphology of the nanostructures. In particular, soft ligands with high affinity for Pd^{II} ions and Pd^0 can both delay nucleation by blocking the coordination of the reducing agent and inhibit nanoparticle aggregation. In contrast, precursors with labile ligand environments promote coordination of the reducing agent and

more facile formation of nanostructures, with ligands of intermediate binding affinity towards Pd facilitating the aggregation-based assembly of nanoparticles into nanodendrites. These ideas are summarized in Figure 3 and were further substantiated by changing the metal by using [Pt(acac)$_2$] as a Pt precursor. As expected, the decomposition of [Pt(acac)$_2$] in only oleylamine yielded Pt dendrites (see Figure S10a in the Supporting Information). A slightly higher temperature was required, which is consistent with the greater thermodynamic and kinetic stability of Pt^{II} complexes compared to Pd^{II} complexes.[12] The addition of either TOP or BTB yielded spherical Pt nanoparticles resistant to aggregation (see Figure S10b,c in the Supporting Information). It is anticipated that this ligand-controlled approach will facilitate the synthesis of new branched nanostructures through aggregation-based assembly, while also providing precursor selection criterion for the design of advanced nanostructures.

Experimental Section

Chemicals and materials: [Pd(acac)$_2$] (99%), Pd(OAc)$_2$, (99.95+%), and [Pd(hfac)$_2$] (99%) were obtained and used as received from Strem Chemicals, Inc. Na_2PdCl_4 (99.995%), oleylamine (OLA, technical grade, 70%), TOP (97%), PPh_3 (99%), and BTB (97%) were purchased from Sigma–Aldrich.

Synthesis: The 10 nm dendrites and 100 nm bundles were prepared as follows: In a typical synthesis, [Pd(acac)$_2$] (0.126 mmol) was mixed in oleylamine (22 mL) to create a pale yellow solution. This solution was heated under continuous stirring from room temperature to 130 °C (ramp rate ca. 20 °C min^{-1}), over the course of which a color change was observed from pale yellow to dark black within 20 min. Small dendrites were collected at 10 min and larger bundles at 1 h. Reaction temperatures ranging from 100 °C to 180 °C yielded similar results, with faster generation of Pd bundles at higher temperatures. Ligand modulation studies followed the same general procedure and incorporated the use of TOP (0.383 mL) or PPh_3 (225.7 mg) and/or BTB (153.53 mg). Pd precursor studies involved the use of [Pd(acac)$_2$], Pd(OAc)$_2$, Na_2PdCl_4, or [Pd(hfac)$_2$] (0.126 mmol). The Na_2PdCl_4 precursor was phase transferred following a previously reported method. Samples were prepared for TEM through collection by centrifugation followed by washing with ethanol three times.

Instrumentation/characterization: TEM was conducted with a JEOL JEM 1010 microscope operating at 80 kV equipped with a ROM CCD camera. High-resolution TEM images were acquired with a JEOL JEM 3500FS microscope using a 4k × 4k Gatan UltraScan 4000 CCD camera. All samples were redispersed in hexanes and drop-casted on Ted Pella copper grids with formvar or carbon coating. The JEOL JEM 3500FS was interfaced with an Oxford INCA dispersive X-ray system for collection of EDX spectra. UV/Vis absorption spectra were recorded with a Varian Cary 100 Bio UV/Vis spectrophotometer using quartz cuvettes and hexanes as a background scan. Powder XRD patterns were obtained with a Scintag diffractometer with Cu Kα radiation.

Received: July 25, 2012
Revised: September 11, 2012
Published online: October 15, 2012

Keywords: aggregation · branched nanoparticles · crystal growth · dendrites · ligand effects

[1] a) B. Lim, Y. Xia, *Angew. Chem.* **2011**, *123*, 78–87; *Angew. Chem. Int. Ed.* **2011**, *50*, 76–85; b) J. Watt, N. Young, S. Haigh, A. Kirkland, R. D. Tilley, *Adv. Mater.* **2009**, *21*, 2288–2293; c) L. Wang, H. Wang, Y. Nemoto, Y. Yamauchi, *Chem. Mater.* **2010**, *22*, 2835–2841; d) L. Wang, Y. Yamauchi, *J. Am. Chem. Soc.* **2009**, *131*, 9152–9153; e) Z. Yin, H. Zheng, D. Ma, X. Bao, *J. Phys. Chem. C* **2009**, *113*, 1001–1005; f) F. Wang, C. Li, L.-D. Sun, C.-H. Xu, J. Wang, J. C. Yu, C.-H. Yan, *Angew. Chem.* **2012**, *124*, 4956–4960; *Angew. Chem. Int. Ed.* **2012**, *51*, 4872–4876; g) L. Zhang, J. Zhang, Z. Jiang, S. Xie, M. Jin, X. Han, Q. Kuang, Z. Xie, L. Zheng, *J. Mater. Chem.* **2011**, *21*, 9620–9625; h) L. M. Bronstein, C. Linton, R. Karlinsey, B. Stein, D. I. Svergun, J. W. Zwanziger, R. J. Spontak, *Nano Lett.* **2002**, *2*, 873–876; i) Y. Zhang, M. Janyasupab, C.-W. Liu, X. Li, J. Xu, C.-C. Liu, *Adv. Funct. Mater.* **2012**, DOI: 10.1002/adfm.201200678; j) L. Wang, C. Hu, Y. Nemoto, Y. Tateyama, Y. Yamauchi, *Cryst. Growth Des.* **2010**, *10*, 3454–3460; k) L. Wang, Y. Yamauchi, *Chem. Mater.* **2009**, *21*, 3562–3569; l) N. Ortiz, S. E. Skrabalak, *Cryst. Growth Des.* **2011**, *11*, 3545–3550.

[2] B. Lim, M. Jiang, P. H. C. Camargo, E. C. Cho, J. Tao, X. Lu, Y. Zhu, Y. Xia, *Science* **2009**, *324*, 1302–1305.

[3] L. Wang, Y. Nemoto, Y. Yamauchi, *J. Am. Chem. Soc.* **2011**, *133*, 9674–9677.

[4] J. Watt, S. Cheong, M. F. Toney, B. Ingham, J. Cookson, P. T. Bishop, R. D. Tilley, *ACS Nano* **2010**, *4*, 396–402.

[5] B. Lim, M. Jiang, T. Yu, P. H. C. Camargo, Y. Xia, *Nano Res.* **2010**, *3*, 69–80.

[6] H. Zheng, R. K. Smith, Y.-w. Jun, C. Kisielowski, U. Dahmen, A. P. Alivisatos, *Science* **2009**, *324*, 1309–1312.

[7] a) H. Hiramatsu, F. E. Osterloh, *Chem. Mater.* **2004**, *16*, 2509–2511; b) Z. Niu, Q. Peng, M. Gong, H. Rong, Y. Li, *Angew. Chem.* **2011**, *123*, 6439–6443; *Angew. Chem. Int. Ed.* **2011**, *50*, 6315–6319; c) S. G. Kwon, T. Hyeon, *Acc. Chem. Res.* **2008**, *41*, 1696–1709; d) A. R. Siedle, L. H. Pignolet, *Inorg. Chem.* **1982**, *21*, 135–141.

[8] Z. Yang, K. J. Klabunde, *J. Organomet. Chem.* **2009**, *694*, 1016–1021.

[9] a) M. F. Casula, Y. Jun, D. J. Zaziski, E. M. Chan, A. Corrias, A. P. Alivisatos, *J. Am. Chem. Soc.* **2006**, *128*, 1675–1682; b) S. G. Kwon, T. Hyeon, *Small* **2011**, *7*, 2685–2702.

[10] Y. Liu, C. Wang, Y. Wei, L. Zhu, D. Li, J. S. Jiang, N. M. Markovic, V. R. Stamenkovic, S. Sun, *Nano Lett.* **2011**, *11*, 1614–1617.

[11] V. Mazumder, S. Sun, *J. Am. Chem. Soc.* **2009**, *131*, 4588–4589.

[12] A. F. Cotton, G. Wilkinson, *Advanced Inorganic Chemistry: A Comprehensive Text*, Wiley, New York, **1980**, p. 951.

